Lawrence Berkeley National Laboratory
Recent Work

Title
Hydrogenated Amorphous Silicon (a-Si:H) Based Gamma Camera - Monte Carlo Simulations

Permalink
https://escholarship.org/uc/item/0f46519w

Authors
Lee, H.
Drewery, J.S.
Hong, W.S.
et al.

Publication Date
1994

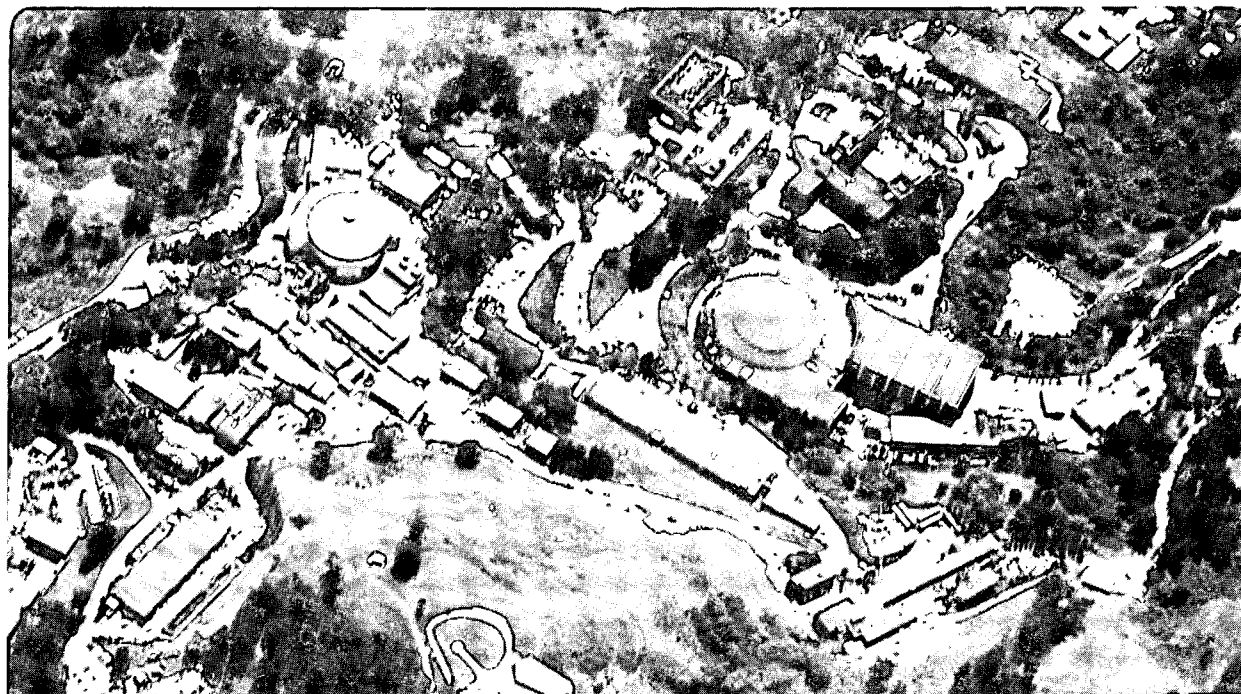# Lawrence Berkeley Laboratory
UNIVERSITY OF CALIFORNIA

Physics Division

To be presented at the SPIE Medical Imaging Conference,
Newport Beach, CA, February 13–18, 1994,
and to be published in the Proceedings

**Hydrogenated Amorphous Silicon (a-Si:H) Based
Gamma Camera – Monte Carlo Simulations**

H. Lee, J.S. Drewery, W.S. Hong, T. Jing, S.N. Kaplan,
A. Mireshghi, and V. Perez-Mendez

January 1994

DISCLAIMER

DISCLAIMER

Hydrogenated Amorphous Silicon (a-Si:H) Based Gamma Camera
- Monte Carlo Simulations

H. Lee, J. S. Drewery, W. S. Hong, T. Jing, S. N. Kaplan,
A. Mireshghi and V. Perez-Mendez

Physics Division
Lawrence Berkeley Laboratory
University of California
Berkeley, CA 94720

January 1994

Hydrogenated amorphous silicon (a-Si:H) based gamma camera - Monte Carlo simulations

Hyoung-Koo Lee, John S. Drewery, Wan-Shick Hong, Tao Jing, Selig N. Kaplan, Ali Mireshghi and Victor Perez-Mendez

Lawrence Berkeley Laboratory, Berkeley, CA 94720

ABSTRACT

A new gamma camera using a-Si:H photodetectors has been designed for the imaging of heart and other small organs. In this new design the photomultiplier tubes and the position sensing circuitry are replaced by 2-D array of a-Si:H p-i-n pixel photodetectors and readout circuitry which are built on a substrate. Without the photomultiplier tubes this camera is light weight, hence can be made portable. To predict the characteristics and the performance of this new gamma camera we did Monte Carlo simulations. In the simulations 128x128 imaging array of various pixel sizes were used. ^{99m}Tc (140keV) and ^{201}Tl (70keV) were used as radiation sources. From the simulations we could obtain the resolution of the camera and the overall system, and the blurring effects due to scattering in the phantom. Using the Wiener filter for image processing, restoration of the blurred image could be achieved. Simulation results of a-Si:H based gamma camera were compared with those of a conventional gamma camera.

1. INTRODUCTION

Utilizing the advantage of large area fabrication, hydrogenated amorphous silicon (a-Si:H) has recently been extensively investigated for x-ray imaging.[1-6] Using similar technologies developed for x-ray imaging, γ-ray imaging with a-Si:H photodetector arrays in nuclear medicine may be possible. γ-ray imaging with a-Si:H arrays were commented in some papers,[1,2,7] but its feasibility for diagnostic imaging has not been investigated thoroughly. In this paper we describe a-Si:H based device which may replace a conventional gamma camera in nuclear medicine and report results from Monte Carlo simulations.

The conventional gamma camera is composed of collimator, scintillator, PMTs and position sensing circuitry. Our camera has a similar detection scheme except that PMTs and position sensing circuitry are replaced by 2-D pixel photodetector array made of a-Si:H and thin film transistor (TFT) readout circuitry. The detector array and readout circuitry are built on the same substrate and the thickness is a few mm at most, hence our camera has less volume and weight than a conventional camera and it is possible to make it portable. This proposed camera can be operated either in event-by-event collection mode or integration mode by appropriate changes in the readout circuits. In the event-by-event collection mode each pixel has a TFT amplifier, and the collection procedure is similar to the conventional cameras using energy selection of the detected γ's. In the integration mode each pixel detector stores the signal charge until the end of the γ scan(2~4min) or the charge can be readout periodically at shorter intervals and the total charge collected per pixel

1

stored on a computer. In this mode high event rate is not a limitation, but the camera will record the scattered γ's as well as the unscattered γ's. In Section 2 details about the device structure and operation scheme are discussed. Using Monte Carlo simulations, for our case, we could obtain and verify various pieces of information such as the main interaction mechanisms, resolution of the camera and scattering effects in the phantom. In Section 3 the results from the simulations are covered. The raw image obtained with the a-Si:H based gamma camera in integration mode is more blurred than the image with the conventional gamma camera due to the scattered γ's in the phantom. If, however, the blurring characteristics are known and the effect is not too severe, the image can be restored by appropriate image deconvolution. Using a Wiener filter the blurring effect due to scattering could be reduced significantly as shown in Section 4.

2. CAMERA STRUCTURE AND OPERATION SCHEME

Fig. 1 shows schematic diagrams of a-Si:H based gamma cameras with two different photodetector configurations. The difference between these two cameras is the existence of the additional storage capacitor on each pixel. These are described in the following subsections.

2.1. Scintillator

CsI(Tl) is an appropriate choice as a scintillator for this gamma camera. CsI(Tl) has a larger light yield than CsI(Na) and is much less hygroscopic.[5,8] Also the emission spectrum of CsI(Tl) matches well the quantum efficiency of a-Si:H photodiode.[5] As discussed in Section 3.1, a CsI(Tl) single crystal of 2~5 mm thickness is enough to detect diagnostic γ-rays.

Type A   Type B

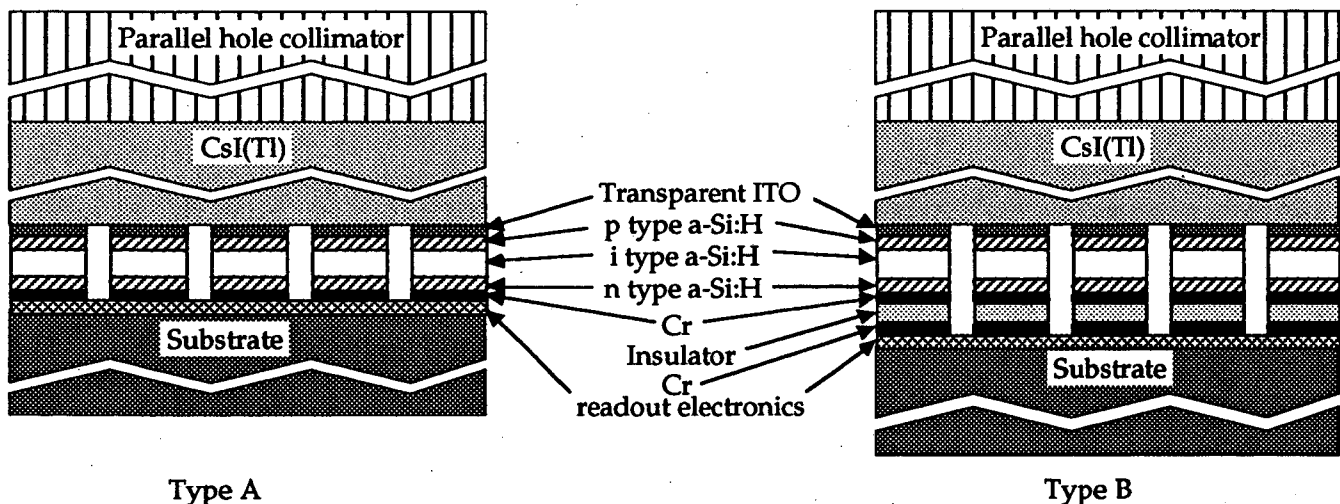Fig. 1   Cross sectional diagram of two a-Si:H based gamma cameras. 5 pixels are drawn for each type. Type A has a conventional p-i-n a-Si:H photodiode array and can be operated either in event-by-event collection mode or integration mode. Type B has additional storage capacitors(Cr-insulator-Cr layers) coupled to p-i-n a-Si:H photodiodes and it can be operated only in integration mode. See text for details.

For a high resolution, if necessary, the crystal can be segmented and the gaps filled with reflecting material. In the simulations unsegmented CsI(Tl) crystal was assumed.

2.2. a-Si:H photodetector arrays

Two kinds of detector structures are possible for the integration mode operation.(Fig. 1) One is the ordinary p-i-n structure (Type A) and the other is p-i-n coupled to an additional storage capacitor for longer integration time (Type B). The thickness of the p-i-n photodiode for both types is ~1μm, which absorbs ~96% of the light incident on the photodiode.[7]

With detectors of type A, in integration mode, the signal charge generated in the p-i-n diode during the imaging period is collected by the internal field of the photodiode and stored on the photodiode itself by the intrinsic capacitance. By closing the TFT switch connected to the photodiode after the integration the signal charge is readout. In this type, however, the charge decays exponentially with time during the integration period. The charge loss is due to the leakage through the photodiode and the OFF-state TFT because of their finite resistances. The charge loss can be reduced by making the TFT smaller and lowering temperature. According to previous reports, decay constants of a few tens of seconds with the photodiode capacitance of 10 ~ 100pF were obtained and a γ-ray imaging with 20 sec integration time was achieved.[1,2] In Nuclear medicine, ~10^6 γ-rays are detected by a gamma camera during ~3 min of acquisition period. With a type A camera with pixel size of 1mm x 1mm x 1μm (105pF), 9 successive readouts with 20 sec integration interval are needed to acquire data for a total acquisition period of 3 min.

In type B the signal charge generated in p-i-n photodiode is stored on the additional storage capacitor.[7] In this case there is no charge leakage because it is blocked by the insulator, but thermally generated dark current in the photodiode is also integrated and stored on the capacitor. The thermally generated background charge can be measured separately and subtracted from the measured signal. If the thermal generation current is too high the background charge will saturate the capacitor and the signal charge cannot be stored with full efficiency. The thermal generation current, however, can be reduced significantly by lowering the ambient temperature as discussed in Reference 7. With a type B camera, 3 min integration times can be achieved.

2.3. Readout electronics and operation schemes

In order to have a high fill factor of the photodetector, it is better to build the readout circuits under the photodetector layers. Depending on the operation scheme there are two methods of signal readout ; (a) image scanning readout and (b) position detecting readout.[9,10] In the integration mode the image scanning readout is appropriate, and in the event-by-event collection mode position detecting readout is suitable. Fig. 2 shows the schematic diagram of readout circuits for each case. With image scanning readout scheme the stored signal on each pixel during the integration period is scanned row-by-row by sequential gate pulses and sent to the external multi-signal processor. In the position detecting readout
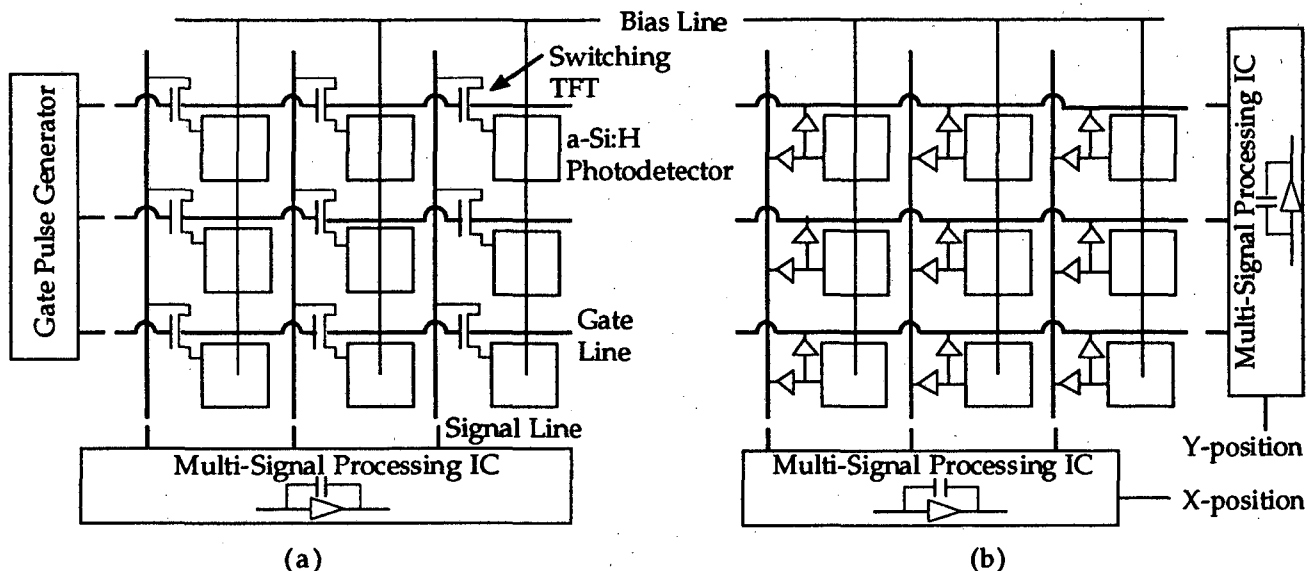
Fig. 2   Schematic diagram of a-Si:H pixel photodetector array with readout electronics.
(a) image scanning readout for integration mode
(b) position detecting readout for event-by-event collection mode

circuits no switching TFT is required, but each pixel has a charge sensitive amplifier which amplifies the low signal charge generated by an event and sends the output to both X and Y output signal lines. This readout scheme can be applied to low event rate such as γ-ray imaging. Whenever a γ-ray is absorbed in the scintillator several a-Si:H pixels will be exposed to the light generated in the scintillator and these pixels will produce signal distributions in X and Y output lines. Then the pixel position which corresponds to the maximum signal both in X and Y direction will be the position of the γ event. By summing all the output signals, the γ energy can be known and, as in the conventional gamma camera, energy selection is possible.

3. MONTE CARLO SIMULATIONS

Monte Carlo simulation programs were made and the performance of the a-Si:H based gamma camera was investigated. In the simulations, integration mode operation was assumed. As sources ^{99m}Tc (E_γ=140keV) and ^{201}Tl (E_γ=70keV) were used and the phantom was made of water. A Picker LEHR parallel-hole collimator was used and the resolution of the collimator as a function of source depth is shown in Fig. 3. An unsegmented CsI(Tl) single crystal was used as a scintillator. The visible light yield from CsI(Tl) was assumed to be 5.2×10^4 photons/1MeV deposited energy[8] and the detector quantum efficiency was set to 70%, which is lower than the reported values of ~80%,[2,3] hence 70% is a conservative assumption.
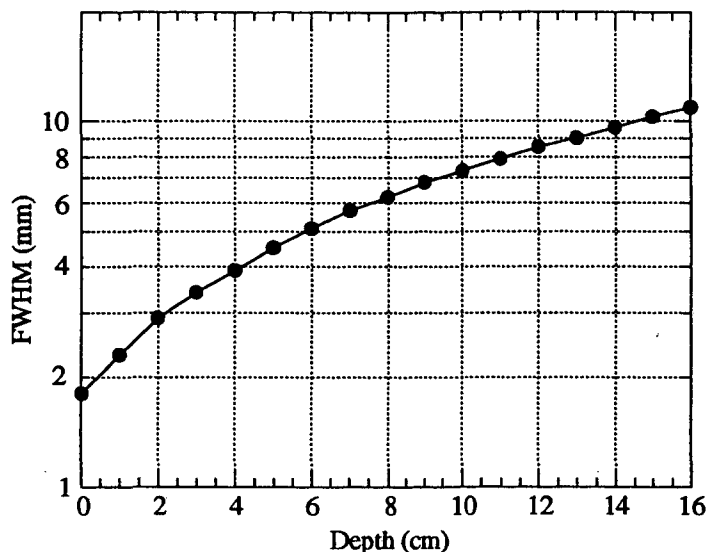
3.1. Detector response - intrinsic resolution

The response of the a-Si:H based gamma camera was tested for varying thicknesses of CsI(Tl) and pixel sizes of the photodetectors. A point source of γ in the air was assumed to emit γ-rays which were incident on the scintillator perpendicular to its surface. As shown in Fig. 4, a 2mm thick CsI(Tl) is sufficient to absorb the γ-rays from ^{201}Tl (99% absorbed), while a thicker CsI(Tl) is needed to absorb the γ-rays from ^{99m}Tc (89% absorbed in 5mm thick CsI(Tl)). Fig. 5 shows the intrinsic resolution of the camera without a collimator. With ^{99m}Tc the resolution is insensitive to CsI(Tl) thickness because of the low cross section of CsI(Tl) at this γ energy. But with γ energy of 70keV from ^{201}Tl, CsI(Tl) has a high cross
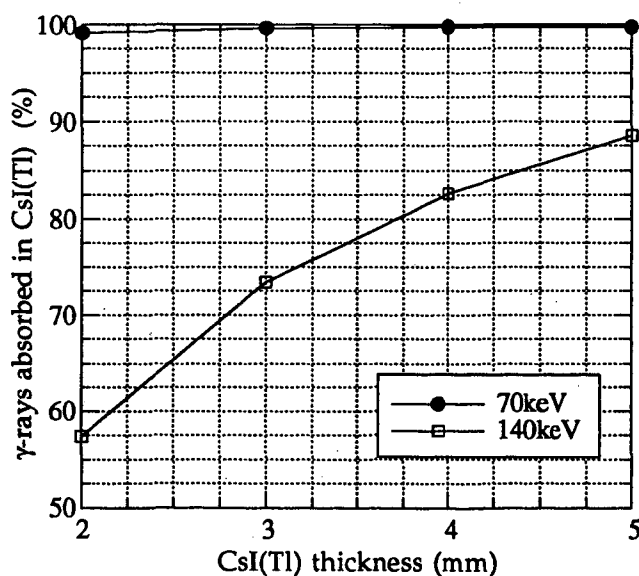

Fig. 4 Percentage of γ-rays absorbed in CsI(Tl) as a function of CsI(Tl) thickness.
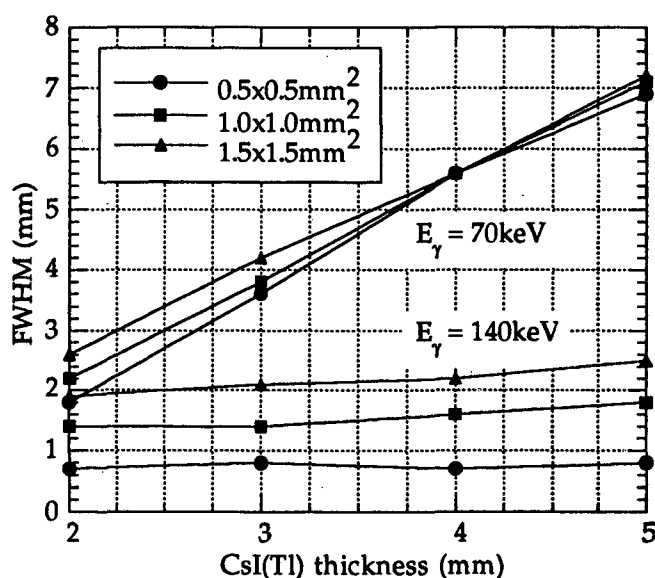
Fig. 5 Intrinsic resolution of a-Si:H based gamma camera as a function of CsI(Tl) thickness with different pixel size.

5

section and most of the interactions occur near top surface, hence the broadening of the visible light is sensitive to the CsI(Tl) thickness. From the above results, a CsI(Tl) crystal of 2mm and 5mm thickness is suitable for 70keV γ-ray imaging and 140keV γ-ray imaging, respectively. As the pixel size is reduced the resolution is better, and with 1mm x 1mm pixel size, the resolution is 2.2mm with 70keV γ and 2mm thick CsI(Tl), and 1.8mm with 140keV γ and 5mm thick CsI(Tl). So the intrinsic resolution of the a-Si:H based gamma camera is better than that of the conventional gamma camera which is 3~4mm. By reducing the pixel size better resolution can be achieved, but there is no need for this because the major contributor to the spatial resolution is the collimator.

3.2. Water phantom

The geometry of the water phantom and the gamma camera is shown in Fig. 6, and the parameters used in the simulations are listed in Table 1. The water phantom is composed of three regions ; hot, warm, and cold. There are no γ sources in the cold region, and the activity of the sources in the warm and hot region is 83.5 kBq/ml and 918.5 kBq/ml, respectively. The distance between the bottom of the warm region and the bottom of the phantom is 7cm, and the hot region is located in the center of the warm region. The bottom of the phantom is in contact with the collimator surface of the gamma camera.
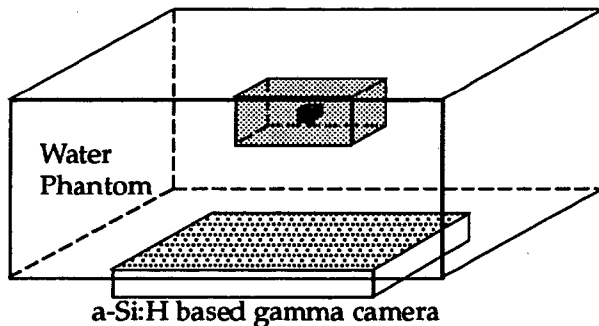
Fig. 6   The geometry of the water phantom with hot, warm and cold sources

■ Hot region

▩ Warm region

□ Cold region

Table 1.   Parameters of the water phantom and the a-Si:H based gamma camera used in simulations

Water phantom	Cold region	size = 30 x 30 x 15 cm^3, activity = 0 kBq/ml
	Warm region	size = 8 x 4 x 4 cm^3, activity = 83.5 kBq/ml
	Hot region	size = 8 x 8 x 8 mm^3, activity = 918.5 kBq/ml
	Distance between bottom of the warm region and bottom of the phantom	7cm
	γ source	^{99m}Tc or ^{201}Tl
Detector	Scintillator	2mm or 5mm thick CsI(Tl)
	Detector area	12.8 x 12.8 cm^2
	Number of pixels	128 x 128 with pixel size of 1 x 1mm^2

3.3. Effect of scattering in the phantom

In order to investigate the scattering effect, the point spread function (PSF) from a point source in the water phantom was simulated. In this simulation the warm and hot regions were removed and a point source with γ energy of 70keV or 140keV was inserted in the phantom. Two different source depths (5cm and 10cm) from the collimator surface were used to investigate the effect of source depth in the phantom. Fig. 7 shows the profiles of the PSF. For 70keV γ-rays, 2mm thick CsI(Tl) was used, and for 140keV, 5mm thickness was used. The PSF is composed of two parts. The peak corresponds to the response of the camera and the FWHM is equal to square root of $R_c^2+R_i^2$, where R_c and R_i is the resolution of the collimator and the scintillator-photodetector, respectively. The exponential tail is due to the scattering in the phantom, which agrees with measurements by others.[11] As shown in Fig. 7 the slope of the tail is dependent on the source depth in the phantom, and as the depth increases the tail broadens. Due to this scattering the projection image of distributed sources will be blurred. Even conventional gamma cameras have scattering effects depending on the size of the energy window and there have been many approaches to remove the scattering effects in PET and SPECT images. Most of the methods, however, require the information about the energy spectra of the detected γ-rays, which is unavailable in a-Si:H based gamma camera in integration mode. However, using deconvolution methods involving Wiener filters, the blurring effect due to the scattering can be largely reduced as discussed in Section 4.2.

3.4. Phantom images

Fig. 8 shows (a) the true object image of the phantom in Fig. 6, (b) the simulated scintigram image with a-Si:H based gamma camera, and (c) the simulated image with a conventional gamma camera. The source used to obtain these images is ^{99m}Tc and the acquisition time is 3min for both images. For the image with a-Si:H based camera, 128 x 128 pixels with 1mm x 1mm pixel size and 5mm thick CsI(Tl) was used. For the conventional
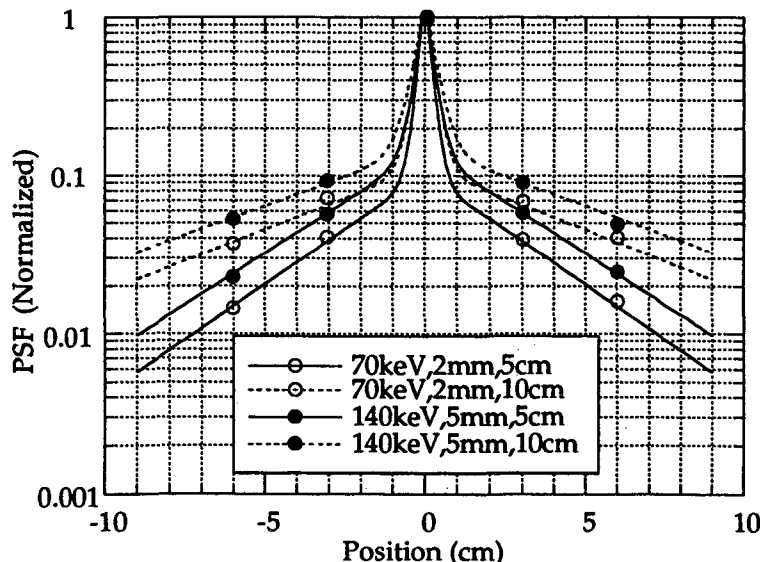

Fig. 7   PSF from a point source in the water phantom with different γ energies and source depths. γ energy : 70keV and 140keV. Source depth : 5cm and 10cm from the collimator surface. Scintillator thickness : 2mm and 5mm

Legend:
- 70keV,2mm,5cm
- 70keV,2mm,10cm
- 140keV,5mm,5cm
- 140keV,5mm,10cm

PSF (Normalized) vs Position (cm)

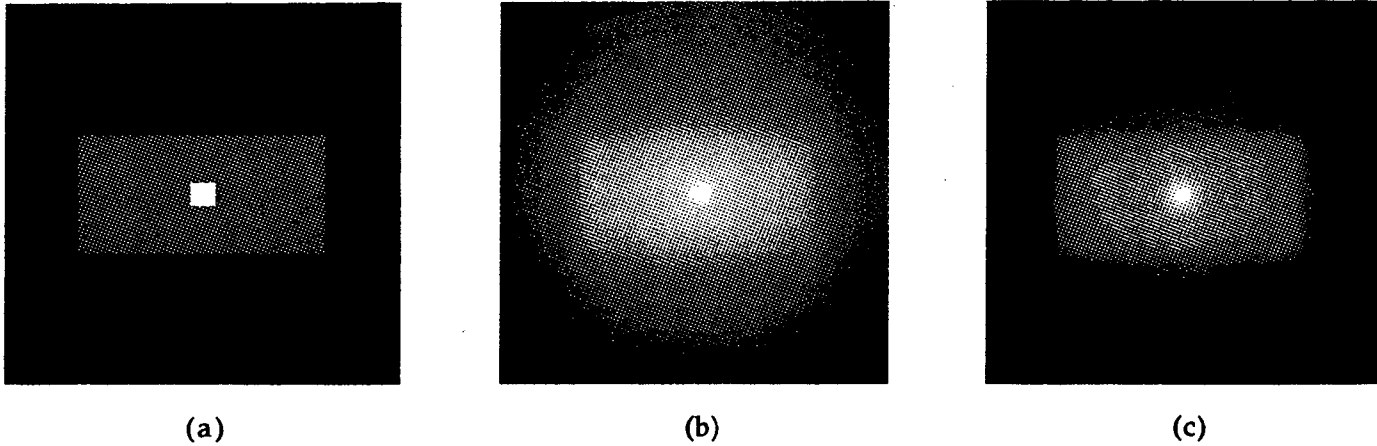|		
(a)	(b)	(c)

Fig. 8   Images from simulations : (a) true object image, (b) simulated image with a-Si:H based gamma camera and (c) simulated image with conventional gamma camera.

camera the same collimator used for a-Si:H based camera was used and the intrinsic resolution of a ZLC 75 Siemens camera,[12] which is 3.8mm, was used. The energy window was set to 10% below the source γ energy, which is a typical value in most cameras. With the same acquisition time the a-Si:H based camera collected more data than the conventional camera because the a-Si:H based camera accepted more scattered γ-rays than the conventional camera. The number of detected γ-rays in the conventional camera image is 9.6×10^5 and in the a-Si:H based camera image is 3.0×10^6. The blurring due to scattering is evident in the image obtained with a-Si:H camera in Fig. 8.

4. NOISE ANALYSES AND IMAGE RESTORATION

4.1. Noise analyses

Noise sources in a-Si:H based gamma camera are (1) noise due to the random process of radiation emission and absorption, (2) fluctuations in the conversion of γ-ray energy to visible light and (3) noise by photodiodes and readout electronics.[4] The image in Fig. 8 (b) contains the noise due to (1) and (2) only. This is count-dependent Poisson noise and generally observed in nuclear medicine images.[13-16] The noise (3) is due to 1/f noise, shot noise and thermal noise in the photodiodes and readout electronics,[4,6,17-19] and this noise may be approximated as a Gaussian noise[4]. Since the current level in our system is very low, the 1/f and shot noises are negligible and the thermal noise due to TFT ON-state resistance will be dominant.[19] This thermal noise can be reduced by lowering the temperature. With the similar pixel size, the mean value of the noise measured by others is ~1.6fC/pixel.[18] The total charge collected to get the image (b) in Fig. 8 is 752 pC and the average is 46fC/pixel. So the noise generated by photodetectors and readout electronics is not important. Moreover this noise can be reduced at lower temperature. To be conservative, a Gaussian noise with a mean value of 2fC/pixel was added to the image Fig. 8 (b) and this image was used as an input image in the image restoration.

4.2. Image restoration

The image obtained with the a-Si:H based gamma camera is degraded by scattering and noise, and this can be mathematically expressed as

$$g(x,y) = h(x,y)*f(x,y) + n(x,y) \qquad (1)$$

where $g(x,y)$ is the obtained image, $f(x,y)$ is the true object image, $h(x,y)$ is the PSF of the system which contains the blurring effect due to camera resolution and scattering in the phantom, and $n(x,y)$ is the noise in the obtained image. "*" in Eq. (1) denotes convolution. A simple inverse filtering in the frequency domain is not adequate to restore the image because it will amplify the noise at high frequencies. A Wiener filter was used to restore the image. The Wiener filter produces the minimum mean-square error between the true object image and the restored image and is often applied to the restoration of nuclear medicine images.[13-15] The Wiener filter in the frequency domain is expressed as

$$WF(u,v) = \frac{1}{H(u,v)} \frac{|H(u,v)|^2}{|H(u,v)|^2 + PN(u,v)/PF(u,v)} \qquad (2)$$

where, $H(u,v)$ is the Fourier Transform of the PSF, and $PN(u,v)$ and $PF(u,v)$ is the power spectrum of the noise and the true object, respectively. The power spectrum of the Poisson noise is a constant equal to the total image count.[13-15] In our case $PN(u,v)$ was set equal to $k*M$, where M is the total image count and k is an adjustment factor. In nuclear medicine

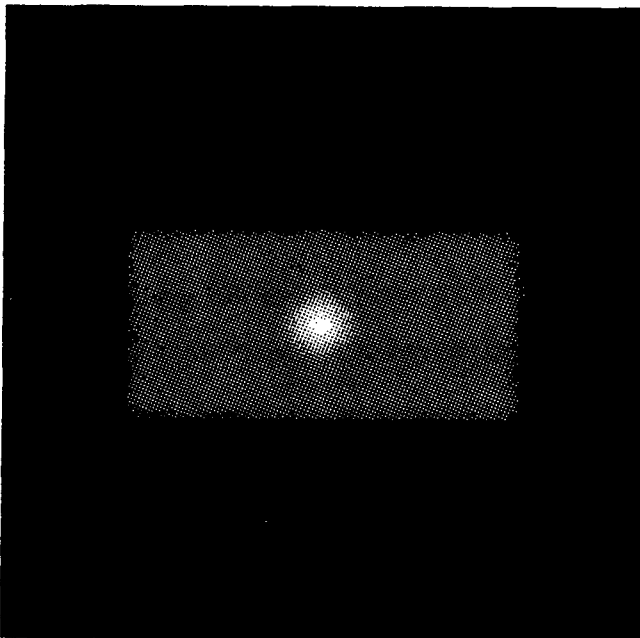|	
———	Simulated image without electronic noise
———	Simulated image with electronic noise
———	Wiener filtered image
—·——·	Simulated image with conventional camera

Fig. 9   Restored image using the Wiener filter. Image in Fig. 8 (b) with added electronic noise was used as the input image.
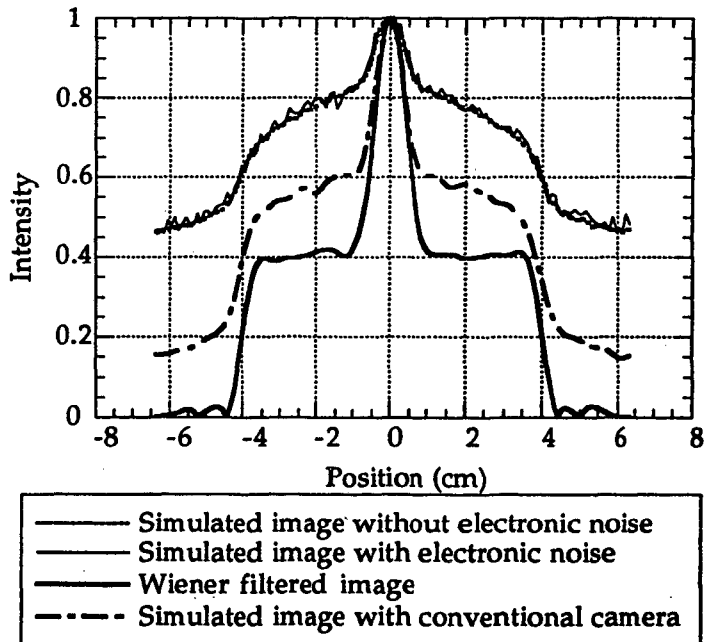
Fig. 10   Profiles of images in x-direction. The intensity is normalized to the maximum count. After restoration, the image obtained with the a-Si:H camera is better than the image obtained by the conventional camera.

9

the information about the true object power spectrum is generally unknown and several methods have been studied to estimate it. We estimated the true object power spectrum from the obtained image by restoration with a Wiener filter with a constant $PN(u,v)/PF(u,v)$ ratio.[20] As shown in Fig. 7 the PSF depends on the source depth, and there cannot be only one PSF for 3-dimensionally distributed sources. Usually the averaged PSF is used in image restoration, hence we used a PSF which is averaged over source depth from 5cm to 11cm. The restored image using the Wiener filter is shown in Fig. 9. The blurring due to scattering is removed and the overall image quality is improved compared to the image in Fig. 8 (b). The image profile in x-direction is compared with those of the image before restoration and the image obtained with a conventional gamma camera in Fig. 10. By the restoration we could obtain a better image with the a-Si:H based camera compared to the image obtained with the conventional gamma camera.

5. DISCUSSION AND CONCLUSION

a-Si:H based gamma camera has been investigated to test the feasibility for use in nuclear medicine. This camera has a different photo-detector structure and readout electronics depending on the operation mode ; integration mode and event-by-event collection mode. The thickness of the scintillator depends on the γ energy and 2~5mm thick CsI(Tl) is adequate for 70~140keV γ-ray imaging with the a-Si:H based gamma camera. The intrinsic resolution obtained from the simulations is ~2mm, which is better than that of the conventional gamma cameras. If necessary, higher intrinsic resolution can be achieved by reducing the pixel size. In the integration mode, the blurring of the image due to scattering is inevitable, but this can be removed by using adequate filter such as the Wiener filter in image processing. Although a strictly correct PSF is unavailable, the error in the image restoration due to mismatch in the PSF is not significant. In Fig. 11 the profiles of the restored images with three different PSFs are compared. The PSFs in Fig. 7 and the averaged
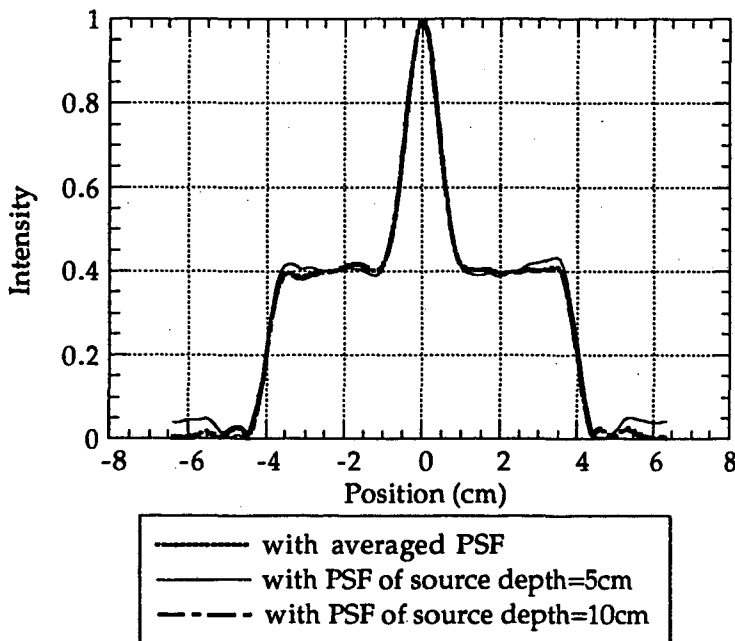
Fig. 11   X-directional profiles of restored images using different PSF. Although PSFs are different depending on the source depth, the resultant images are not sensitive to the mismatch in the PSF.

Legend:
- with averaged PSF
- with PSF of source depth=5cm
- with PSF of source depth=10cm

PSF were used. Although the slopes of the tails in the PSF shapes in Fig. 7 are different depending on the source depth, the restoration process is not sensitive to the mismatch in the PSF as shown in Fig. 11. After image restoration we could obtain better images with the a-Si:H based gamma camera than the conventional gamma camera. According to this study, γ-ray imaging in nuclear medicine with a-Si:H arrays is possible using similar technologies developed for x-ray imaging with a-Si:H photodiode arrays.

6. ACKNOWLEDGMENTS

7. REFERENCES

1. I. Fujieda, S. Nelson, P. Nylen, R. A. Street and R. L. Weisfield, "Two operation modes of 2D a-Si sensor arrays for radiation imaging," J. Non-Crystalline Solids, Vol. 137 & 138, pp. 1321-1324, 1991.

2. I. Fujieda, S. Nelson, R. A. Street and R. L. Weisfield, "Radiation imaging with 2D a-Si sensor arrays," IEEE Trans. Nucl. Sci., Vol. NS-39, PP. 1056-1062, 1992.

3. L. E. Antonuk, J. Yorkston, W. Huang, J. Boudry, E. J. Morton and R. A. Street, "Large area, flat-panel a-Si:H arrays for x-ray imaging," SPIE Vol. 1896, Medical Imaging 1993 : Physics of Medical Imaging, pp. 18-29, 1993.

4. N. H. Clinthorne, "Are hydrogenated amorphous silicon arrays usable for tomographic imaging?," Presented at IEEE Nuclear Science Symposium and Medical Imaging Conference, San Francisco, November 1993.

5. I. Fujieda, G. Cho, J. S. Drewery, T. Gee, T. Jing, S. N. Kaplan, V. Perez-Mendez, D. Wildermuth and R. A. Street, "X-ray and charged particle detection with CsI(Tl) layer coupled to a-Si:H photodiode layers," IEEE Trans. Nucl. Sci., Vol. NS-38, pp. 255-262, 1991.

6. R. A. Street, S. Nelson, L. Antonuk and V. Perez-Mendez, "Amorphous silicon sensor arrays for radiation imaging," Mat. Res. Soc. Symp. Proc., Vol. 192, pp.441-452, 1990.

7. H. Lee, G. Cho, J. S. Drewery, W. S. Hong, T. Jing, S. N. Kaplan, A. Mireshghi, V. Perez-Mendez and D. Wildermuth, "New a-Si:H photo-detectors for long-term charge storage," Mat. Res. Soc. Symp. Proc., Vol. 297, pp. 1023-1028, 1993.

8. I. Holl, E. Lorenz and G. Mageras, "A measurement of the light yield of common inorganic scintillators," IEEE Trans. Nucl. Sci., Vol. NS-35, pp. 105-109, 1988.

9. G. Cho, J. S. Drewery, W. S. Hong, T. Jing, S. N. Kaplan, H. Lee, A. Mireshghi, V. Perez-Mendez and D. Wildermuth, "Signal readout in a-Si:H pixel detectors," IEEE Trans. Nucl. Sci., Vol. NS-40, pp. 323-327, 1993.

10. G. Cho, V. Perez-Mendez, M. Hack and A. Lewis, "Charge-sensitive poly-silicon TFT amplifiers for a-Si:H pixel particle detectors," Mat. Res. Soc. Symp. Proc., Vol. 258, pp. 1181-1186, 1992.

11. P. Msaki, B. Axelsson and S. A. Larsson, "Some physical factors influencing the accuracy of convolution scatter correction in SPECT," Phys. Med. Biol., Vol. 34, pp. 283-298, 1989.

12. Siemens Inc., "ZLC 370/750 series : collimator performance specifications," Gamma camera catalogue.

13. M. A. King, P. W. Doherty and R. B. Schwinger, "A Wiener filter for nuclear medicine images," Med. Phys., Vol. 10, pp. 876-880, 1983.

14. M. T. Madsen, "A method for obtaining an approximate Wiener filter," Med. Phys., Vol. 17, pp. 126-130, 1990.

15. B. C. Penney, S. J. Glick and M. A. King, "Relative importance of the error sources in Wiener restoration of scintigrams," IEEE Trans. Medical Imaging, Vol. 9, pp. 60-70, 1990.

16. M. J. Belanger, A. B. Dobrzeniecki and J. C. Yanch, "Noise characteristics of a SPECT simulation system," Presented at IEEE Nuclear Science Symposium and Medical Imaging Conference, San Francisco, November 1993.

17. G. Cho, S. Qureshi, J. S. Drewery, T. Jing, S. N. Kaplan, H. Lee, A. Mireshghi, V. Perez-Mendez and D. Wildermuth, "Noise in a-Si:H p-i-n detector diodes," IEEE Trans. Nucl. Sci., Vol. NS-39, pp. 641-644, 1992.

18. I. Fujieda, S. Nelson, R. A. Street and R. L. Weisfield, "Characteristics of a-Si pixel arrays for radiation imaging," Mat. Res. Soc. Symp. Proc., Vol. 219, pp. 537-542, 1991.

19. I. Fujieda, R. A. Street, R. L. Weisfield, S. Nelson, P. Nylen, V. Perez-Mendez and G. Cho, "High sensitivity readout of 2D a-Si image sensors," Jpn. J. Appl. Phys., Vol. 32, pp. 198-204, 1993.

20. T. R. Miller and K. S. Sampathkumaran, "Design and application of finite impulse response digital filters," Eur. J. Nucl. Med., Vol. 7, pp. 22-27, 1982.